RSC Advances

PAPER

View Article Online
View Journal | View Issue

Cite this: *RSC Adv.*, 2023, **13**, 30243

Preparation of mesoporous chitosan iron supported nano-catalyst for the catalyzed oxidation of primary amine to imine†

Lan Wu,[ab] Yang Liu,[ab] Zhenhua Li,[*ab] Jinhua Liang,[*ac] Lei Geng,[a] Li Chen[a] and Zhengping Dong[*c]

Received 7th August 2023
Accepted 30th September 2023

DOI: 10.1039/d3ra05357a

rsc.li/rsc-advances

Supported nano-catalysts with environmental sustainability and high catalytic performance are of great research interest for sustainable catalysis. In this article, a supported nano-catalyst, FeA-NC, with high catalytic performance was prepared by anchoring the transition metal iron onto nitrogen-doped porous carbon materials using chitosan as a raw material. Scanning electron microscopy (SEM), X-ray diffraction (XRD) and Fourier transform infrared spectroscopy (FT-IR) measurement results demonstrated that the obtained catalyst has an excellent mesoporous structure, and that the element Fe is evenly distributed. The support contains abundant N atoms, which can provide sufficient anchoring points for Fe and form Fe–N_x groups with Fe, improving the catalytic activity of the catalyst. Additionally, the FeA-NC with a porous structure can also enhance the mass transfer of reactants to improve the reaction efficiency. In addition, the prepared catalyst was used to catalyze the conversion of primary amines to the corresponding imines. The results showed that the direct oxidation of primary amines to the corresponding imines can be catalyzed by using air as an oxygen source and distilled H_2O as a solvent under atmospheric pressure at 90 °C. Finally, the selectivity and stability of the as-prepared catalyst were also verified.

Introduction

Imines, which are considered to be key intermediates in the synthesis of refined drugs, natural products and fine chemicals, are widely used in agricultural, pharmaceutical, and synthetic chemistry and the fine chemical industry.[1,2] In industrial and academic laboratories, imines can be produced through various traditional thermal catalytic processes. Generally, imines are prepared by condensation reactions between primary or secondary amines and aldehydes or ketones using noble metal (Pd, Ru, and V) complexes as Lewis-acid catalysts.[3,4] However, the frequent use of precious metal catalysts in the common synthesis processes will increase pollution of the environment and waste scarce resources, which is a serious problem in light of the strict requirements of modern society for green and sustainable development.[5–7]

In the past decade, great progress has been made in the exploration of imine synthesis routes, including cross-coupling of amines and alcohols, oxidation self-coupling of primary amines, oxidation of secondary amines[1–5] and photocatalytic selective oxidation of primary amine to imide.[8] The new method of directly coupling the excess metal onto a carbon material through the oxidative dehydrogenation of primary amines has attracted great attention due to its environmental and economic advantages.[9,10] Carbon nanocatalysts, due to their efficient catalytic performance and environmental sustainability in catalyzing the oxidation of benzylamine and reactive coupling to form *N*-benzylbenzylamine (*N*-imine), have shown great promise in practical applications.[11]

It is essential to prepare supported nano-catalysts with high catalytic performance and environmental sustainability for the synthesis of imines.[13] Metal-supported nanocatalysts are prepared from transition metals (such as Fe, Co, Ni, Mn, Cu) highly dispersed on nitrogen-doped porous carbon materials.[14] Supported nanocatalysts based on the transition metal iron, with low cost and excellent catalytic performance, are ideal candidates for catalyst materials.[15] The activity of metal catalysts depends on the exposure of the active metal sites, and reducing the size of the metal nanoparticles is an ideal strategy to improve their catalytic activity.[27] However, when the size of the iron nanoparticles is small, it is easy for them to agglomerate in the catalytic reaction, which leads to an increase in the

[a]*College of Chemical Engineering, Northwest Minzu University, Lanzhou, Gansu 730030, PR China. E-mail: lizhh02006@163.com; Fax: +86 931 4512932; Tel: +86 931 4512932*

[b]*Key Laboratory of Environment-Friendly Composite Materials of the State Ethnic Affairs Commission, Gansu Provincial Biomass Function Composites Engineering Research Center, Key Laboratory for Utility of Environment-Friendly Composite Materials and Biomass, University of Gansu Province, Lanzhou 730030, China*

[c]*State Key Laboratory of Applied Organic Chemistry, Laboratory of Special Function Materials and Structure Design of the Ministry of Education, College of Chemistry and Chemical Engineering, Lanzhou University, Lanzhou 730000, PR China. E-mail: dongzhp@lzu.edu.cn*

† Electronic supplementary information (ESI) available. See DOI: https://doi.org/10.1039/d3ra05357a

size of the iron nanoparticles and a decrease in their performance. Studies have shown that a suitable combination of metal and support, the design of an efficient supported metal nanoparticle catalyst, and the use of metal–support interaction, can improve the dispersion of metal nanoparticles and effectively reduce the agglomeration of nanoparticles during the catalytic process.[28] Ma *et al.*[16] successfully synthesized a supported nano-catalyst in which the non-noble metal Fe was supported on nitrogen-doped porous carbon derived from biomass, which was used to efficiently catalyze the oxidation of primary amine to imine with air as an oxidizing agent. Chen *et al.*[17] reported a supported nano-catalyst with a mesoporous medium, homogeneous metal NPs and abundant oxygen vacancies for the synthesis of imines.

Due to the excellent abundance, low toxicity, excellent activity, and stability of nitrogen-doped porous carbon materials, they have received great attention.[12,13] In the process of preparing nitrogen-doped porous carbon-supported nanocatalysts, the selection of nitrogen-doped carbon materials is a crucial step. Biomass is the most abundant renewable resource on earth[18] and is widely used in biomedicine,[19] fuel[20] and catalysis.[21] Renewable biomass has the advantages of high absorption,[22] unique structure, abundant resources, biodegradability and low cost. Therefore, using renewable biomass as a nitrogen-doped carbon material is a good choice.[23,24] Therefore, in this work, chitosan is used as a support for the preparation of supported nanocatalysts.

The introduction of transition metals is another key factor in the preparation of supported catalysts. Primo *et al.*[11] catalyzed the oxidation of primary amine to imine using graphene oxide as a catalyst. However, because the transition metal was not introduced into the catalyst, the catalyst is used in the reaction process is very large, which limits the practical application of the catalyst to a large extent. Wu *et al.*[25] achieved significant electrocatalytic hydrogen evolution activity by grafting graphene nanosheet catalysts embedded with carbon nanotubes containing Co nanoparticles. Chen *et al.*[26] embedded Ni/Co bimetallic nanoparticles into nitrogen-doped carbon nanotube (NCNT) tips, which exhibited stronger amine adsorption and weaker photogenerated hydrogen adsorption than the monometallic-based catalysts, and were more favorable for the dehydrogenation activation of primary amines and generation of imines. Therefore, in this work, a high performance supported nano-catalyst (FeA-NC) was prepared by using the transition metal Fe anchored on a nitrogenous doped porous carbon material derived from chitosan, and was used to catalyze the direct oxidation of primary amines to imines at 90 °C under atmospheric pressure, with air as an oxygen source and distilled H_2O as a solvent. In summary, a method for the environmentally friendly synthesis of imines was provided.

Experiment

Chemical materials

Chitosan, *N*,*N*-dimethylformamide (DMF), dimethyl sulfoxide (DMSO), 1,4-dioxane, acetic acid (CH_3COOH), ferric nitrate ($Fe(NO_3)_3 \cdot 9H_2O$), and methylbenzene were purchased from Shanghai Aladdin Biochemical Technology Co., Ltd. Hydrochloric acid (HCl), sodium hydroxide (NaOH), and tetrahydrofuran (THF) were purchased from Sinopharm Chemical Reagent Co., Ltd. (China). Deionized H_2O was prepared in the laboratory. All chemicals were used without further purification.

Experimental apparatus

Scanning electron microscopy (SEM, Thermo AperoS) and transmission electron microscopy (TEM, FEI Talos F200s) were used to analyze the morphological and structural characteristics of the prepared materials. The crystal structure of the catalyst was determined using powder X-ray diffraction (PXRD, Rigaku MiniFlex 600). The functional groups were analyzed using FT-IR (Bruker VERTEX 70). X-ray photoelectron spectroscopy (XPS, PerkinElmer PHI-5702) was used to analyze the valence states of the different elements on the surface of the material. The actual metal content of the catalyst was determined using inductively coupled plasma optical emission spectrometry (ICP-AES). The Brunauer–Emmett–Teller (BET, 3H-2000PSA2) method was used to analyze the specific surface area and pore size distribution. Gas chromatography (GC-2014 + AFSC, 230C) and gas chromatography mass spectrometry (GC-MS, Agilent 5977E) were used to detect the selectivity of the oxidation of the primary amine to corresponding imines.

Preparation of Fe-NC

First, 2 g of chitosan was dispersed in acetic acid solution (1 wt%) and stirred at room temperature for 24 h. Then, 0.1 g $Fe(NO_3)_3 \cdot 9H_2O$ was added, and the mixture was stirred at room temperature for 2 h until completely uniform. The above solution was dropped into a NaOH (4 M) solution using a syringe to induce the spontaneous gelation of chitosan into porous beads. The product was soaked in alkaline solution for 5 h and cleaned once with distilled H_2O, and then dried in a vacuum drying oven at 60 °C for 24 h. The prepared Fe–CS was transferred to a porcelain boat and then placed in a tube furnace, which was gradually heated to 800 °C at a heating rate of 5 °C min^{-1} under an inert atmosphere (N_2), and calcined for 2 h.

Preparation of FeA-NC

The Fe-NC obtained in the above steps was placed in 50 mL HCl (1 M) solution and stirred at 60 °C for 12 h, after which the product was collected by pumping and filtering. After washing it with distilled H_2O until neutral, the collected catalyst was placed in a vacuum drying oven and dried at 60 °C for 24 h.

Preparation of NC-800

First, 2 g of chitosan was dispersed in an acetic acid solution (1 wt%) and stirred at room temperature for 24 h. The above solution was dropped into a NaOH (4 M) solution with a syringe to induce the spontaneous gelation of chitosan into porous beads. After soaking the product in alkaline solution for 5 h, the solution was washed once with distilled H_2O. The product was then dried in a vacuum drying oven at 60 °C for 24 h. After that, the obtained material was transferred to a porcelain boat and

placed in a tube furnace, which was gradually heated to 800 °C at a heating rate of 5 °C min^{-1} under an inert atmosphere (N_2) and calcined for 2 h.

Experiments on the catalytic oxidation of primary amines to imines

Typically, 0.5 mmol of primary amine and 50 mg of catalyst were placed in a 10 mL round-bottomed flask with 5 mL of solvent. Then, in the condensation tube, the whole reaction system was stirred in an oil bath at 90 °C under an air atmosphere until the specified time. Finally, the used catalyst was collected by centrifugation for subsequent use.

Recovery experiment

Catalysts reused before the fifth cycle were centrifuged at 12 000 rpm for 3 minutes. They were then repeatedly washed with anhydrous ethanol three times and dried in a vacuum drying oven at 30 °C for 24 h.

Results and analysis

In this study, supported nanocatalysts with highly dispersed iron nanoparticles were prepared on nitrogen-doped porous carbon materials. As shown in Scheme 1, firstly, chitosan and ferric nitrate were uniformly dispersed in acetic acid (1 wt%) and then dropped into NaOH solution (4 M) with a syringe to induce the spontaneous gelation of chitosan into porous beads. Secondly, the dried hydrogel was calcined in a tube furnace under N_2 at 800 °C for 2 h to obtain the Fe-NC material. Finally, the obtained material Fe-NC was etched with hydrochloric acid (1 M) to obtain the catalyst FeA-NC, in which Fe-NPs existed in small size.

In order to conveniently observe the structure of the prepared supported nanocatalysts, FeA-NC was analyzed using transmission electron microscopy. As shown in Fig. 1(a), Fe NPs (red circle) were present on the nitrogen-doped porous carbon material, indicating that after etching with hydrochloric acid (1 M), the large-size Fe NPs were etched into small-size Fe NPs. Additionally, as shown in Fig. 1(b), the average diameter of the existing Fe NPs was about 15 nm. In addition, the corresponding element mapping shown in Fig. 1(c) confirmed that the elements C, N, O and Fe contained in the supported nanocatalyst FeA-NC were uniformly distributed.

The XRD patterns of NC-800, Fe-NC, and FeA-NC are shown in Fig. 2(a). It can be seen from curve 1 that the nitrogen-doped porous carbon material prepared in our study has a certain crystallinity, and there is no significant loss of the crystallinity in Fe-NC (curve 2), which showed that the incorporation of Fe NPs had no effect on the crystallinity of NC-800. However, compared with the previous two materials, Fe-NC showed significant loss of crystallinity, which may be caused by the hydrochloric acid (1 M) etching in order to increase the pores in the nitrogen-doped porous carbon material and obtain Fe-NP-loaded catalysts. In addition, no Fe peaks were observed in curve 3, which may be due to the low actual Fe content in the target catalyst FeA-NC. The large broad peak in curve 3 is because the support loses its original crystal structure after being etched with hydrochloric acid.

Fig. 2(b) presents the FT-IR spectra of chitosan, NC-800 and FeA-NC. As shown in Fig. 2(b), the peak centered at 1500–500 cm^{-1} is the vibration caused by the C–N band participating in the skeleton vibration of the molecule. Meanwhile, the peaks at 1129 cm^{-1} and 1135 cm^{-1} are attributed to the stretching and deformation vibrations of –OH, while those at 1568 cm^{-1} and 1680 cm^{-1} are attributed to the stretching vibrations of NH and carbonyl (C═O–NHMe), respectively. In addition, the peak at 1825 cm^{-1} can be attributed to the deformation vibrations of –CH_2 and –CH_3. The strong peak at 1440 cm^{-1} can be ascribed to the bending vibration of –CH. The weak peak at 879 cm^{-1} can be assigned to the –NH bending vibration.

The wide-range XPS spectrum (Fig. 3(a)) shows that the prepared catalyst FeA-NC contains four elements: C, N, O, and Fe. The high-resolution C 1s spectrum displays two peaks at 284.6 eV and 290.0 eV, which are assigned to C–C and C–O, respectively (Fig. 3(b)). As shown in Fig. 3(c), the high-resolution N 1s spectra of the two samples can be deconvolved to pyridine nitrogen, graphene nitrogen, and nitrogen oxide, respectively, clearly demonstrating that N atoms have been successfully introduced into the carbon lattice. However, the N peaks of FeA-NC are shifted to lower binding energy [pyridine nitrogen (398.0 eV), graphene nitrogen (400.8 eV), nitrogen oxide (402.5 eV)] than those of NC-800. This may be due to the interaction between the Fe NPs and N atoms embedded in the carbon framework to form Fe-N_x. The high-resolution Fe 2p spectrum of FeA-NC (Fig. 3(d)) shows two peaks centered at 711.2 eV and 714.1 eV. The peaks at 711.2 eV and 714.1 eV are

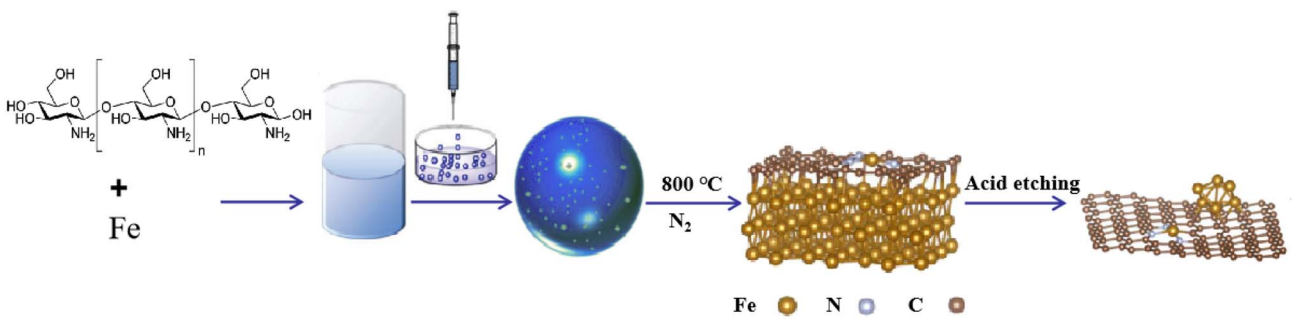

Scheme 1 Preparation process of the FeA-NC catalyst.

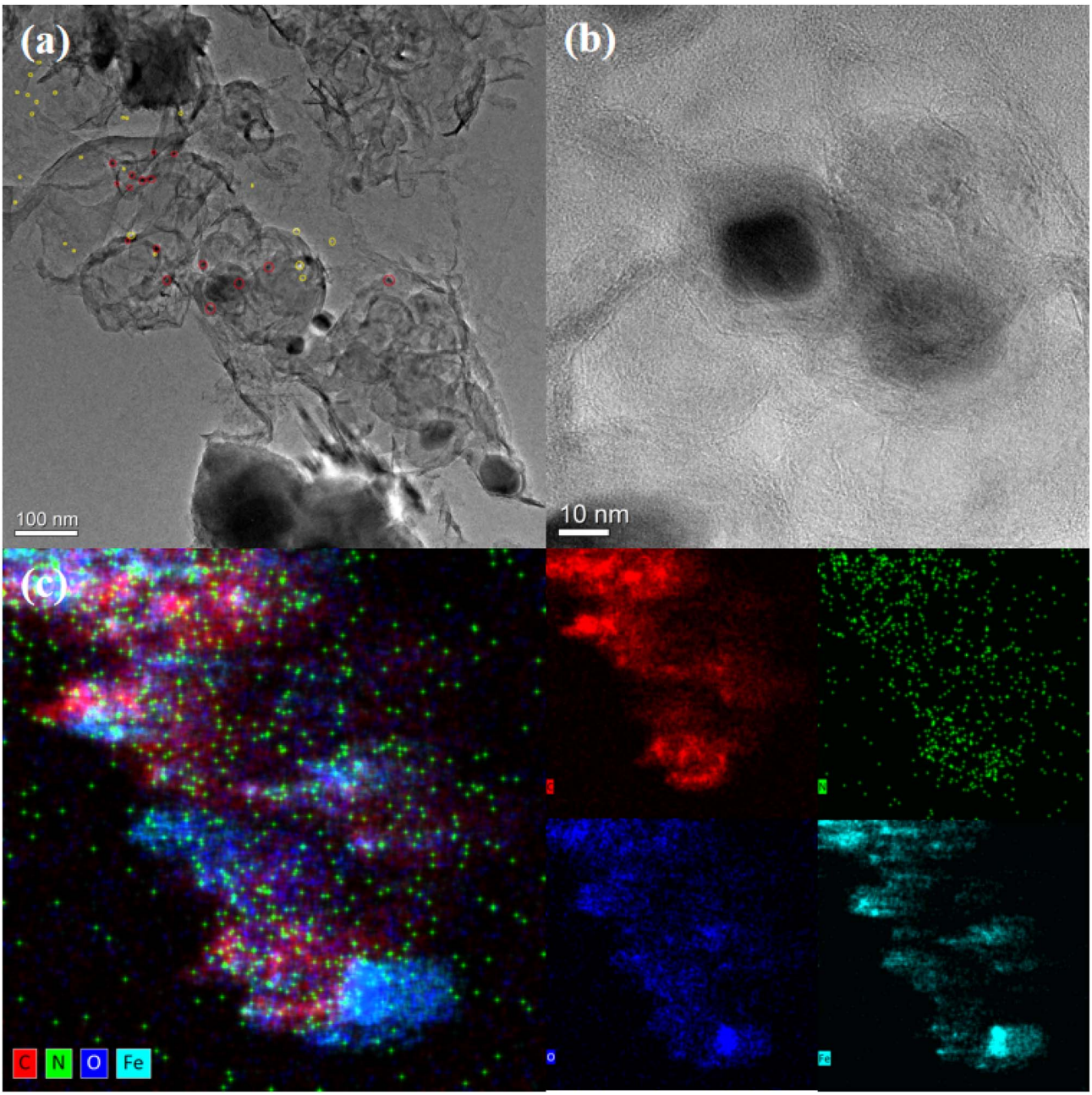

Fig. 1 (a) and (b) TEM images of FeA-NC (red circles are Fe NPs); (c) HAADF-STEM image of C, N, O, Fe for FeA-NC.

attributed to the Fe $2p_{1/2}$ and Fe $2p_{3/2}$ orbitals of Fe^{2+} and Fe^{0}, respectively, where the co-existing Fe^{2+} may be due to the presence of Fe–N bonds. From the XPS spectra, it can be found that the peak of Fe is weaker than those of C, O and other elements, which may be due to the low content of Fe introduced. The actual loading of Fe in FeA-NC as measured using ICP-OES was 0.98 mmol%, as shown in Table 1.

The specific surface area and pore size distributions of the synthetic materials are shown in Fig. 4 and Table 2. As shown in Fig. 4(a), both NC-800 and Fe-NC exhibit N_2 adsorption–desorption curves of both type I and type IV, with specific surface areas of 5.889 $m^2\ g^{-1}$ and 17.517 $m^2\ g^{-1}$, respectively, indicating that both microporous and mesoporous structures exist in these two materials. As shown in curve 3 of Fig. 4(a), FeA-NC shows a N_2 adsorption–desorption curve of type I, with a specific surface area of 219.664 $m^2\ g^{-1}$, indicating the existence of mesoporous structures in this material, which is due to the conversion of micropores into mesoporous pores after etching with hydrochloric acid (1 M). The pore size distribution of the prepared catalyst FeA-NC is shown in Fig. 4(b), and the average pore size of FeA-NC is about 8.414 nm.

Under specific conditions, oxygen in the air is used as the oxygen source, and the direct oxidation of benzylamine to imine under atmospheric pressure was used as the model reaction to detect the catalytic activity of the prepared supported nanocatalyst (FeA-NC). The reaction conditions of the model reaction

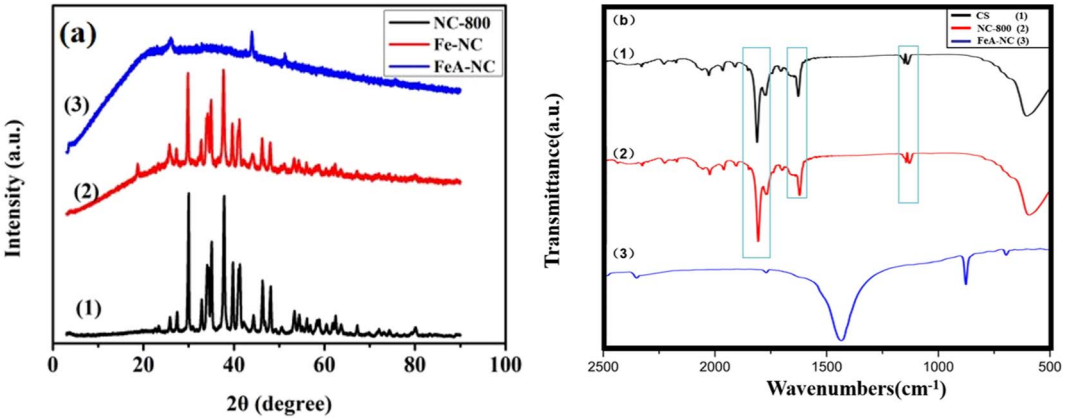

Fig. 2 (a) XRD patterns of NC-800 (1), Fe-NC (2), and FeA-NC (3); (b) FTIR spectra of chitosan (1), NC-800 (2), and FeA-NC (3).

were optimized, and the experimental data are shown in Table 2.

Firstly, the temperature of the reaction greatly affects the catalytic effect of the reaction. As shown in Table 3, entries 1 and 2, when the reaction temperature was 50 °C or 70 °C, the conversion rate of benzylamine to imine was only 36.0% and 83.7%, respectively. However, when the reaction temperature was 90 °C or 100 °C, the conversion rate increased to 95.9% and 97.0%, respectively (Table 3, entries 3 and 4). Although the conversion rate of benzylamine was the highest at 100 °C, compared with 90 °C, the conversion rate did not increase significantly with this increase of temperature and the selectivity decreased. In order to save energy, 90 °C was chosen as the reaction temperature.

Table 1 Determination of Fe content in fresh and reused FeA-NC by ICP-OES

Sample	Fe (mmol%)
Fresh	0.98
Reused	0.89

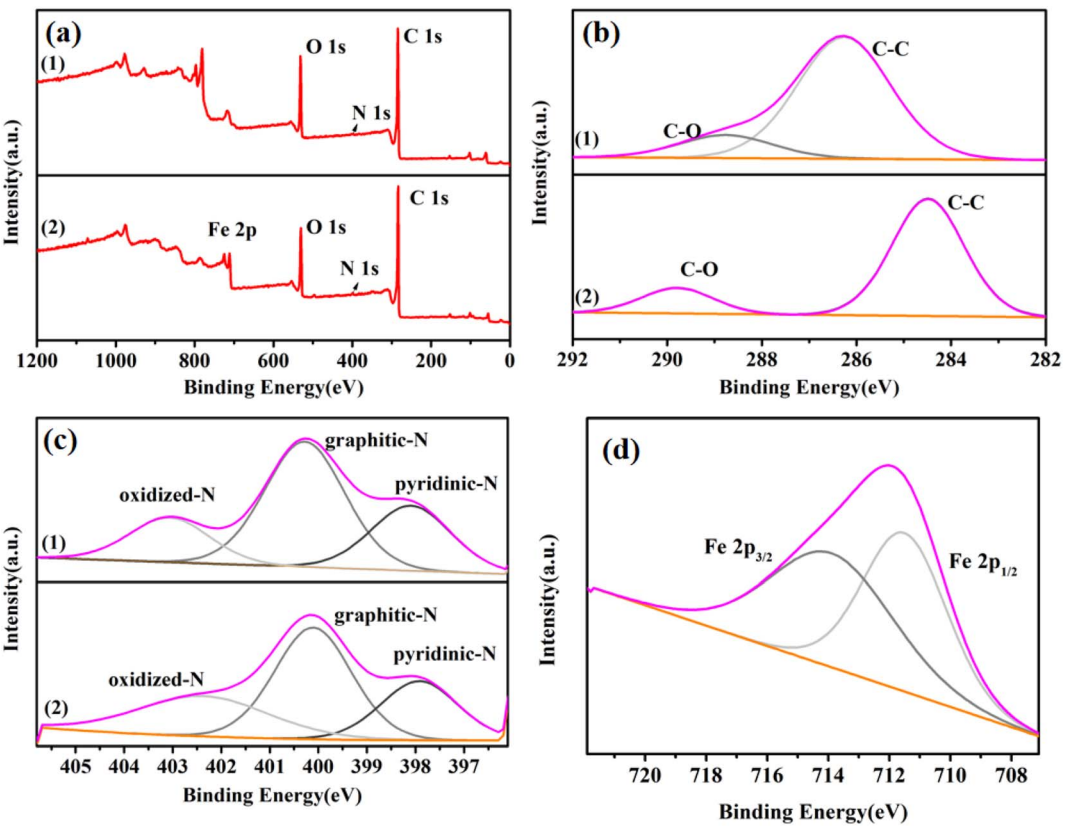

Fig. 3 (a) Wide-range XPS spectra of NC-800 (1) and FeA-NC (2). (b) High-resolution spectra of C 1s, (c) high-resolution spectrum of N 1s, and (d) high-resolution spectrum of Fe in FeA-NC.

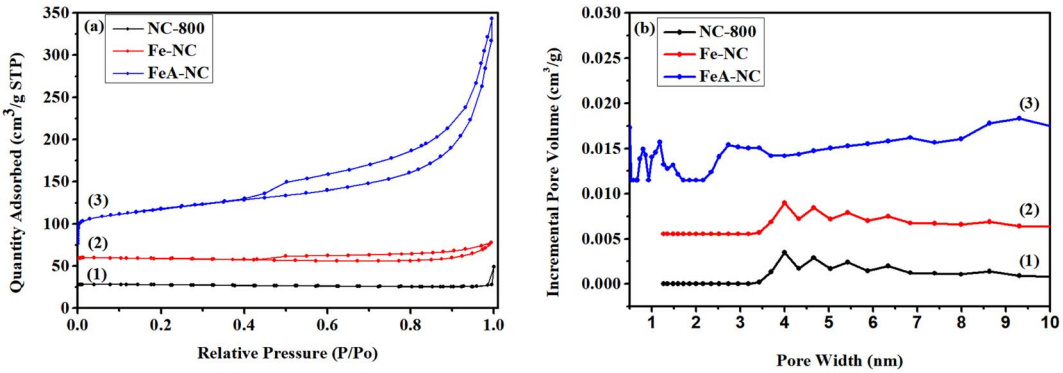

Fig. 4 (a) BET diagrams of NC-800, Fe-NC and FeA-NC; (b) the corresponding aperture distribution curves.

Table 2 BET specific surface area and pore structure characterization parameters of the catalysts studied

Sample	BET surface area ($m^2\ g^{-1}$)	Pore volume ($cm^3\ g^{-1}$)	Average pore size (nm)
NC-800	5.889	0.023	4.023
Fe-NC	17.517	0.035	4.191
FeA-NC	219.664	0.331	8.414

Secondly, the solvent used in the reaction is also a key factor affecting the catalytic effect.[29] Different reaction solvents were added to explore the influence of different solvents on the reaction (Table 3, entries 3 and 5–8). The results show that under the same conditions, when using H_2O as the solvent, the conversion of the reaction reaches 95.9%, which is obviously higher than using other solvents. A possible reason is that H_2O is a proton-type polar solvent, which can spontaneously lose hydrogen ions, associate with solute molecules *via* hydrogen bonds or form coordination cations, and the lone pair electrons after the loss of hydrogen ions can stabilize the cation of the system. As a polar solvent, H_2O can cause the polar solute molecule benzylamine to form an unstable active intermediate, which has a catalytic effect, can promote the formation of ions, and is conducive to single-molecule reaction; thus, it promotes a high conversion rate and high selectivity. DMSO, DMF, 1,4-dioxane, toluene are aprotic solvents. They have a solvent effect on the solute molecules, so the solvent has good selectivity, but the conversion rate is low. Thus, H_2O was selected as the solvent for this reaction in order to better convert primary amine to imine.

Table 3 Optimum conditions for benzylamine oxidation

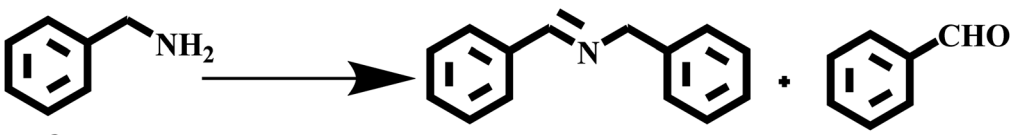

a b c

Entry	Catalyst	Solvent	*t*/h	*T*/°C	Conv./%	Sel. (**b**)/%	Sel. (**c**)/%
1[a]	FeA-NC	H_2O	24	50	36.0	>99	—
2[a]	FeA-NC	H_2O	24	70	83.7	>99	—
3[a]	FeA-NC	H_2O	24	90	95.9	95.2	4.8
4[a]	FeA-NC	H_2O	24	100	97.0	93.5	6.5
5[b]	FeA-NC	Toluene	24	90	51.8	>99	—
6[b]	FeA-NC	DMF	24	90	37.1	>99	—
7[b]	FeA-NC	DMSO	24	90	22.1	>99	—
8[b]	FeA-NC	1,4-Dioxane	24	90	47.7	>99	—
9[c]	—	H_2O	24	90	2.8	>99	—
10[c]	NC-800	H_2O	24	90	10.9	>99	—
11[c]	Fe-NC	H_2O	24	90	16.9	>99	—
12[d]	GO	CH_3CN	5	75	42.0	88.0	1.0
13[e]	Ru-MIC	Toluene	15	80	90	>99	—

[a] Reaction conditions: 0.5 mmol benzylamine, 50 mg catalyst, 5 mL H_2O, air, 24 h. [b] Reaction conditions: 0.5 mmol benzylamine, 50 mg catalyst, 5 mL solvent, 90 °C, air, 24 h. [c] Reaction conditions: 0.5 mmol benzylamine, 50 mg catalyst, 5 mL H_2O, 90 °C, air, 24 h. [d] Reaction conditions: 0.5 mmol benzylamine, 100 mg catalyst, 5 mL solvent, 75 °C, air, 5 h.[11] [e] Reaction conditions: 0.5 mmol benzylamine, 1 mol% catalyst, 2 mL toluene, 80 °C, O_2 (balloon), 15 h.[29]

Table 4 Substrate expansion[a]

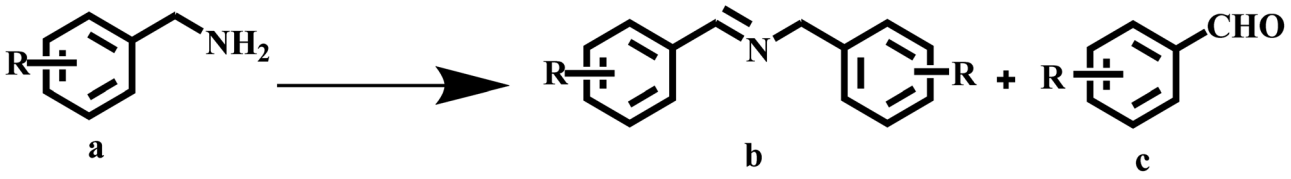

Entry	Substrate	Conv. (%)	**b** sel. (%)	**c** sel. (%)
1	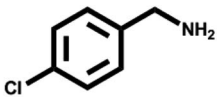	>99	90.0	10.0
2	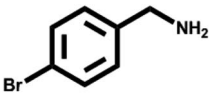	>99	>99	—
3	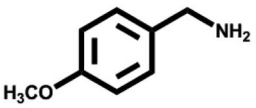	>99	46.2	53.8
4	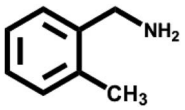	>99	90.8	9.2
5	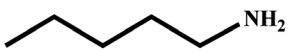	>99	87.9	12.1

[a] Reaction conditions: 0.5 mmol primary amine, 50 mg catalyst, 5 mL H_2O, 90 °C, air, 24 h.

Under the optimized reaction conditions (90 °C, H_2O), the catalytic activity of the model reaction was explored using the three prepared materials and without the use of a catalyst. Benzylamine is difficult to convert to imine without a catalyst (Table 3, entry 9). However, after adding NC-800 to the reaction system, the conversion rate can be increased to 10.9% (Table 3, entry 10), indicating that nitrogen-doped porous carbon materials play a certain driving role in the reaction process. Secondly, when the reaction was catalyzed the catalyst Fe-NC with Fe NPs added, the conversion rate of primary amine was only increased to 16.9% (Table 3, entry 11), indicating that the introduction of Fe had a certain effect on the reaction, but the catalytic activity was not high. Surprisingly, when the target catalyst FeA-NC was used to catalyze the reaction, the conversion rate increased rapidly to 95.2% (Table 3, entry 3), indicating that after the use of hydrochloric acid to etch Fe-NC, not only can the gaps in the nitrogen-doped porous carbon material be expanded to facilitate mass transfer, but it is also possible to etch the large-size Fe NPs into small-size Fe NPs to catalyze the reaction efficiently. Additionally, the TON under these conditions is 48.96, implying that the catalyst exhibits good activity. In addition, our catalyst was compared with some in previously published articles;[11,29] although GO (Table 3, entry 12) can catalyze the reaction, the catalyst has a higher mass lower conversion rate (42.0%) and poor selectivity (88.0%). When Ru-MIC is used as the catalyst, the reaction temperature (80 °C) is slightly lower than that for FeA-NC; however, Ru is a noble metal, and toluene is used as the solvent (Table 3, entry 13). Therefore, the use of FeA-NC as the catalyst, H_2O as a green solvent, air as the oxygen source, and a reaction temperature of 90 °C under atmospheric pressure were used as the optimal conditions for the conversion of benzylamine to imine.

Various primary amines were tested as reactants under the optimized conditions to further understand the versatility of the FeA-NC catalysts. In the case of the two tested compounds containing halogen atoms (3-chlorobenzylamine and 3-

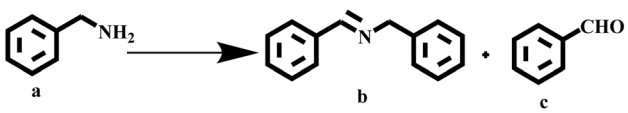

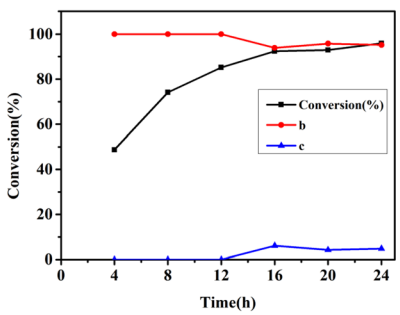

Fig. 5 Product distribution after different reaction times.

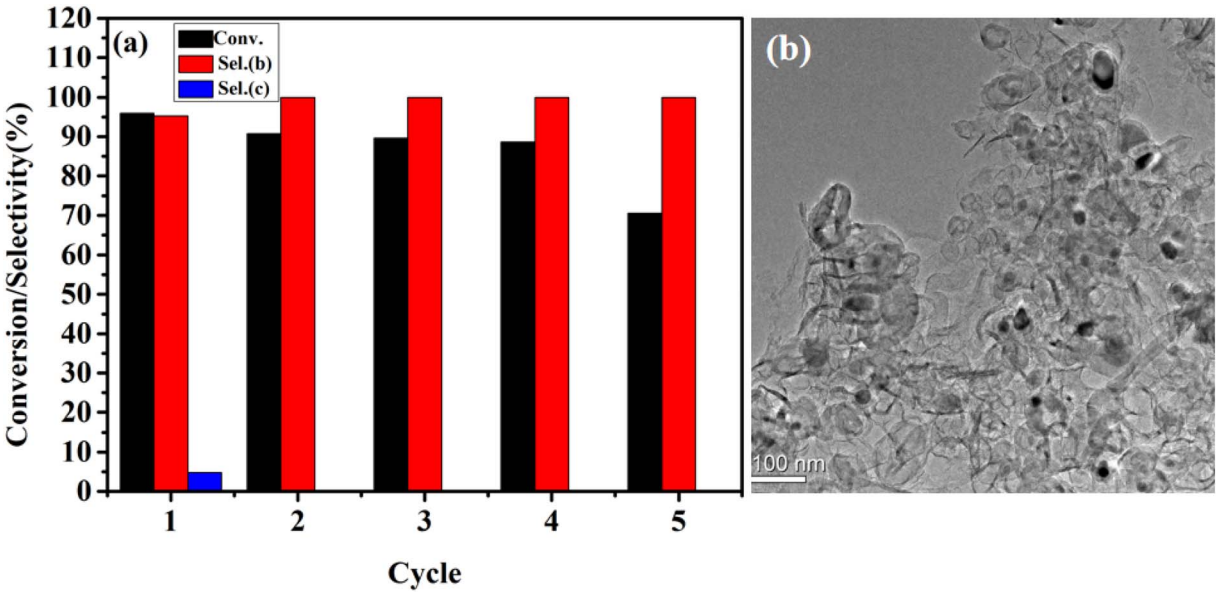

Fig. 6 (a) Cycling experiment of FeA-NC in the catalytic oxidation of primary amine; (b) TEM image of FeA-NC after the fifth use.

bromobenzylamine), the conversion rate of primary amine can reach more than 99% without any dehalogenation, and the selectivity is also very high, at 90% and 99%, respectively (Table 4, entries 1 and 2). Secondly, for both benzylamines containing electron-withdrawing groups (3-chlorobenzylamine and 3-bromobenzylamine) and a benzylamine containing an electron-donating group (2-methylbenzylamine, Table 4, entry 4), the primary amine can be efficiently converted to the corresponding imine. Moreover, the catalyst also had good catalytic activity for a fatty amine (1-aminopentane) (Table 4, entry 5). Surprisingly, although 3-methoxybenzylamine is also a benzylamine containing electron-withdrawing groups, and the groups are at the *para*-positions, the selectivity of its conversion to the corresponding imine is only 46.2% (Table 4, entry 3). This may be due to the fact that methoxy is an electron-donating group, which is more difficult to carry out mass transfer than other electron-withdrawing groups, resulting in a lower electrophilicity of the imine intermediate; thus, the selectivity of the conversion to the corresponding imine is lower.[30] In general, the prepared target catalyst FeA-NC can be applied to a certain range of substrates.

In order to better understand the reaction process, the reaction time and the distribution of the target product were carefully monitored (Fig. 5). As can be seen from Fig. 5, when the reaction was carried out for 4 h, the conversion rate was 48.7%, and the products at this time were all imines (99%). When the reaction was carried out for 12 h, the conversion of benzylamine was 85.0%, and the selectivity of imine was 98.2%; at this point, the by-product benzaldehyde (1.8%) began to appear. With the extension of the reaction time (24 h), benzylamine was successfully converted (95.9%); the selectivity of the target product was 95.2%, and that of the by-product was 4.8%.

In order to evaluate the durability of FeA-NC catalyst, it was collected after the primary amine catalytic oxidation experiment for reuse. As shown in Fig. 6(a), the prepared catalyst can be reused five times while maintaining its catalytic activity and selectivity, indicating its high durability. In addition, the actual Fe content of the FeA-NC catalyst after repeated use five times was 0.89 mmol%, which was different from the actual Fe content of the fresh catalyst (0.98 mmol%). Thus, at the fifth reuse, the catalytic activity plummeted to 70.5%, possibly due to the aggregation of Fe NPs during the collection process (Fig. 6(b)).

Conclusions

The supported catalyst FeA-NC was prepared by highly dispersing Fe-NPs onto nitrogen-doped porous carbon materials. Under atmospheric pressure, primary amine can be catalyzed to imine directly using air as an oxygen source through the action of this catalyst. Additionally, a range of different primary amines can be effectively converted to the corresponding imines with high yield and good selectivity. The results showed that the catalytic activity of the nitrogen-doped porous carbon materials can be effectively improved by introducing Fe. It is worth noting that after etching with hydrochloric acid (1 M), the pores of the nitrogen-doped porous carbon are expanded to facilitate mass transfer of the initial reactants, and the large-sized Fe-NPs are also etched into small-sized Fe-NPs for the direct catalytic oxidation of primary amines to imines. Adding Fe to nitrogen-doped porous carbon can reduce the use of Fe, thereby reducing environmental pollution and avoiding resource waste, and Fe can combine with N to form Fe–N_x species to improve catalytic activity. In summary, the acid-etched catalyst FeA-NC was reasonably designed in this work, which provides a path for the future research and development of other supported heterogeneous catalysts.

Conflicts of interest

The authors declare no conflicts of interest.

Acknowledgements

This work is supported by the Key Program of Natural Science Foundation of Gansu Province (No. 22JR5RA178), the Gansu Key Research and Development Program (No. 22YF7FA172), the Fundamental Research Funds for the Central Universities (No. 31920230168), Lanzhou Chengguan District Science and Technology Plan Project (No. 2022JSCX0009), Gansu Province University Teacher Innovation Fund Project (No. 2023B-049) and the Natural Science Foundation of Gansu Province (No. 21JR1RA198).

References

1 P. Ji, K. Manna, Z. Lin, X. Feng, A. Urban, Y. Song and W. Lin, *J. Am. Chem. Soc.*, 2017, **139**, 7004–7011.
2 B. S. Takale, X. Feng, Y. Lu, M. Bao, T. Jin, T. Minato and Y. Yamamoto, *J. Am. Chem. Soc.*, 2016, **138**, 10356–10364.
3 S. Kobayashi, Y. Mori, J. S. Fossey and M. M. Salter, *Chem. Rev.*, 2011, **111**, 2626–2704.
4 S. Kobayashi and H. Ishitani, *Chem. Rev.*, 1999, **99**, 1069–1094.
5 B. Yan, W.-C. Li and A.-H. Lu, *J. Catal.*, 2019, **369**, 296–301.
6 H. Huang, J. Huang, Y.-M. Liu, H.-Y. He, Y. Cao and K.-N. Fan, *Green Chem.*, 2012, **14**, 930–934.
7 R. V. Jagadeesh, H. Junge and M. Beller, *ChemSusChem*, 2015, **8**, 92–96.
8 J. Zhou, X. Li, X. Ma, W. Sheng and X. Lang, *Appl. Catal., B*, 2021, **296**, 120368–120377.
9 J. Long, K. Shen and Y. Li, *ACS Catal.*, 2017, **7**, 275–284.
10 X. Lang, H. Ji, C. Chen, W. Ma and J. Zhao, *Angew. Chem., Int. Ed.*, 2011, **50**, 3934–3937.
11 A. Primo, M. Puche, O. D. Pavel, B. Cojocaru, A. Tirsoaga, V. Parvulescu and H. García, *Chem. Commun.*, 2016, **52**, 1839–1842.
12 S. Li, B. Dong, Y.-Y. Zhang and P. Xu, *ChemistrySelect*, 2020, **5**, 14307–14311.
13 S. K. Singh, K. Takeyasu, B. Paul, S. K. Sharma and J. Nakamura, *Sustainable Energy Fuels*, 2021, **5**, 820–827.
14 Y.-S. Wei, M. Zhang, R. Zou and Q. Xu, *Chem. Rev.*, 2020, **120**, 12089–12174.
15 S.-S. Zhang, Y.-C. Zheng, Z.-W. Zhang, S.-Y. Chen, H. Xie, B. Shu, J.-L. Song, Y.-Z. Liu, Y.-F. Zeng and L. Zhang, *Org. Lett.*, 2021, **23**, 5719–5723.
16 Z. Ma, S. Liu, N. Tang, T. Song, K. Motokura, Z. Shen and Y. Yang, *ACS Catal.*, 2022, **12**, 5595–5604.
17 W.-T. Chen, S. Han, Z.-H. Dai, Y.-X. Fu, M.-S. Sun, Z.-M. Li, Y. Zhou and D.-J. Tao, *J. Porous Mater.*, 2023, **30**, 705–712.
18 J. Popp, S. Kovács, J. Oláh, Z. Divéki and E. Balázs, *New Biotechnol.*, 2021, **60**, 76–84.
19 D. Li, Y. Wang, W. Huang and H. Gong, *Front. Mater.*, 2023, **10**, 1058050–1058064.
20 L. K. Palniandy, L. W. Yoon, W. Y. Wong, S.-T. Yong and M. M. Pang, *Energies*, 2019, **12**, 2477–2492.
21 S. Elanthikkal, H. H. Mohamed and N. A. Alomair, *Arabian J. Chem.*, 2023, **16**, 104522–104535.
22 C. Pennesi, A. Amato, S. Occhialini, A. T. Critchley, C. Totti, E. Giorgini, C. Conti and F. Beolchini, *Sci. Rep.*, 2019, **9**, 16763–16774.
23 L. Sun, Y. Gong, D. Li and C. Pan, *Green Chem.*, 2022, **24**, 3864–3894.
24 J. Garcia-Cardona, I. Sirés, M. Mazzucato, R. Brandiele, E. Brillas, F. Alcaide, C. Durante and P. L. Cabot, *Electrochim. Acta*, 2023, **442**, 141911–141924.
25 Z. Chen, R. Wu, Y. Liu, Y. Ha, Y. Guo, D. Sun, M. Liu and F. Fang, *Adv. Mater.*, 2018, **30**, 1802011–1802021.
26 Y. Chen, D. Sun, L. Du, Y. Jiao, W. Han and G. Tian, *ACS Appl. Mater. Interfaces*, 2022, **14**, 24425–24434.
27 F. Yang, D. Liu, Y. Zhao, H. Wang, J. Han, Q. Ge and X. Zhu, *ACS Catal.*, 2018, **8**, 1672–1682.
28 Z. Xie, T. Zhang and Z. Zhao, *ACS Appl. Nano Mater.*, 2021, **4**, 9353–9360.
29 S. Yadav, S. Pal, N. K. Pal, N. U. Din Reshi, S. Pal and J. K. Bera, *Appl. Organomet. Chem.*, 2022, e6594–e6606.
30 F. Zhang, X. Li, X. Dong, H. Hao and X. Lang, *Chin. J. Catal.*, 2022, **43**, 2395–2404.